Bioactive Materials 6 (2021) 2029–2038

Contents lists available at ScienceDirect

Bioactive Materials

journal homepage: www.sciencedirect.com/journal/bioactive-materials

Restoration of electrical microenvironment enhances bone regeneration under diabetic conditions by modulating macrophage polarization

Xiaohan Dai [a,b,c,1], Boon Chin Heng [d,1], Yunyang Bai [c], Fuping You [e], Xiaowen Sun [b], Yiping Li [a], Zhangui Tang [a], Mingming Xu [c,***], Xuehui Zhang [b,f,**], Xuliang Deng [c,f,*]

[a] Hunan Key Laboratory of Oral Health Research & Hunan 3D Printing Engineering Research Center of Oral Care & Hunan Clinical Research Center of Oral Major Diseases and Oral Health & Xiangya Stomatological Hospital & Xiangya School of Stomatology, Central South University, Changsha, 410008, PR China
[b] Department of Dental Materials & Dental Medical Devices Testing Center, Peking University School and Hospital of Stomatology, Beijing, 100081, PR China
[c] Department of Geriatric Dentistry, Peking University School and Hospital of Stomatology, Beijing, 100081, PR China
[d] Central Laboratory, Peking University School and Hospital of Stomatology, Beijing, 100081, PR China
[e] Institute of Systems Biomedicine, Department of Immunology, School of Basic Medical Sciences, Beijing Key Laboratory of Tumor Systems Biology, Peking University Health Science Center, Beijing, 100191, PR China
[f] National Engineering Laboratory for Digital and Material Technology of Stomatology, NMPA Key Laboratory for Dental Materials, Beijing Laboratory of Biomedical Materials & Beijing Key Laboratory of Digital Stomatology, Peking University School and Hospital of Stomatology, Beijing, 100081, PR China

ARTICLE INFO

Keywords:
Electrical microenvironment
Diabetes
Ferroelectric nanocomposites
Bone regeneration
Macrophage polarization

ABSTRACT

Macrophage-mediated inflammation compromises bone repair in diabetic patients. Electrical signaling cues are known to regulate macrophage functions. However, the biological effects of electrical microenvironment from charged biomaterials on the immune response for regulating osteogenesis under diabetic conditions remain to be elucidated. Herein the endogeneous electrical microenvironment of native bone tissue was recapitulated by fabricating a ferroelectric $BaTiO_3$/poly (vinylidene fluoridetrifluoroethylene) (BTO/P(VDF-TrFE)) nanocomposite membrane. *In vitro*, the polarized $BaTiO_3$/poly (vinylidene fluoridetrifluoroethylene) (BTO/P(VDF-TrFE)) nanocomposite membranes inhibited high glucose-induced M1-type inflammation, by effecting changes in cell morphology, M1 marker expression and pro-inflammatory cytokine secretion in macrophages. This led to enhanced osteogenic differentiation of human bone marrow mesenchymal stem cells (BM-MSCs). *In vivo*, the biomimetic electrical microenvironment recapitulated by the polarized nanocomposite membranes switched macrophage phenotype from the pro-inflammatory (M1) into the pro-healing (M2) phenotype, which in turn enhanced bone regeneration in rats with type 2 diabetes mellitus. Mechanistic studies revealed that the biomimetic electrical microenvironment attenuated pro-inflammatory M1 macrophage polarization under hyperglycemic conditions by suppressing expression of AKT2 and IRF5 within the PI3K-AKT signaling pathway, thereby inducing favorable osteo-immunomodulatory effects. Our study thus provides fundamental insights into the biological effects of restoring the electrical microenvironment conducive for osteogenesis under DM conditions, and offers an effective strategy to design functionalized biomaterials for bone regeneration therapy in diabetic patients.

1. Introduction

Diabetes mellitus (DM) is one of the most common metabolic diseases and is anticipated to increase to over 590 million cases by 2035 worldwide [1,2]. Following the onset of DM, patients often suffer from an increased incidence of bone fracture, delayed bone healing and high

Peer review under responsibility of KeAi Communications Co., Ltd.
* Corresponding author. Department of Geriatric Dentistry, Peking University School and Hospital of Stomatology, Beijing, 100081, PR China.
** Corresponding author. Department of Dental Materials & Dental Medical Devices Testing Center, Peking University School and Hospital of Stomatology, Beijing, 100081, PR China.
*** Corresponding author. Department of Geriatric Dentistry, Peking University School and Hospital of Stomatology, Beijing, 100081, PR China.
E-mail addresses: anniemmx@126.com (M. Xu), zhangxuehui@bjmu.edu.cn (X. Zhang), kqdengxuliang@bjmu.edu.cn (X. Deng).
[1] These authors contributed equally to this work.

https://doi.org/10.1016/j.bioactmat.2020.12.020
Received 22 September 2020; Received in revised form 20 December 2020; Accepted 21 December 2020

risk of bone graft implantation failure [3,4]. Several mechanisms involved in diabetes-associated bone repair abnormalities are generally recognized, including increased levels of pro-inflammatory mediators, inhibition of angiogenesis and impaired osteoblast function [5–7]. Intensive studies have revealed that the following therapeutic intervention approaches could facilitate bone healing under diabetic conditions, for example the local application of anti-inflammatory cytokines [8], hyperbaric oxygen therapy [9] or implantation of isogenic adult stem cells (ASCs) [10]. Hence, it is imperative to develop an effective implant modification strategy to minimize these adverse effects and improve osteogenesis in DM patients.

As a chronic inflammatory disease, the diabetic wound often remains abnormally stagnated at the early pro-inflammatory stage of the healing process, characterized by elevated expression levels of inflammatory factors including IL-1β and IL-6 [5,6]. A growing number of studies have demonstrated that elevated glucose levels often trigger excessive inflammatory activation of macrophages, suggesting that hyperglycemia hinders the transition from the pro-inflammatory to anti-inflammatory state during the healing process [11,12]. Because it is well-established that macrophages are key regulators of the immune response and healing process, intensive research have been focused on developing novel modifications of implant materials for modulating macrophage function to promote osteogenesis [13,14]. In response to microenvironmental signals, macrophages can either display pro-inflammatory M1 phenotype (classically-activated) or pro-healing M2 phenotype (alternatively-activated). These findings point to osteoimmunomodulatory biomaterials as a promising strategy that can enhance osteogenesis under hyperglycemic conditions, by promoting macrophage polarization to the M2 phenotype.

It is reported that the electrical microenvironment plays an important role in bone regeneration [15,16]. Studies have reported that electrical signaling cues could modulate macrophage migration, phagocytic activity and cytokine production [17,18]. However, little attention has been focused on the biological effects of restoration of electrical microenvironment on macrophage polarization and subsequent osteogenesis under DM conditions. Therefore, in this study, the biomimetic electrical microenvironment mimicking native bone extracellular matrix (ECM) was recapitulated by polarized $BaTiO_3$/poly (vinylidene fluoridetrifluoroethylene) (BTO/P(VDF-TrFE)) ferroelectric nanocomposites, which has been shown to have excellent osteogenic effects in our previous study [19]. As illustrated in Scheme 1, the electrical dipoles of BTO NPs are reoriented. Consequently, opposite charges are generated on both sides of membranes after corona poling treatment. When the negative charge side of the nanocomposite membrane is implanted inward covering the bone defect area, it can form an enclosed electrical microenvironment with the negatively charged bone wall. Within such a restored electrical microenvironment, M1 macrophages under hyperglycemic conditions could be induced into the M2 phenotype with reduced IL-6 secretion, through inhibition of AKT2-IRF5 signaling, thereby creating a favorable osteo-immunomodulatory environment. Consequently, endogenous bone marrow mesenchymal stem cells (BM-MSCs) can be induced to differentiate into osteoblasts and rapid bone regeneration is exhibited within the osteo-immunomodulatory microenvironment induced by the polarized nanocomposite membranes.

2. Materials and methods

2.1. Fabrication and characterization of BTO/P(VDF-TrFE) nanocomposite membranes

The BTO/P(VDF-TrFE) nanocomposite membranes were prepared using the solution casting method as described by our previous study [19]. Firstly, BTO NPs (Alfa Aesar, Heysham, UK) were stirred in 0.01 mol/L of dopamine hydrochloride (Alfa Aesar, Heysham, UK) aqueous solution for 12 h at 60 °C. Then, to form a stable suspension, powders consisting of the modified BTO NPs and P(VDF-TrFE) (Arkema, Paris, France) co-polymers were uniformly dispersed in N, N - dimethylformamide (DMF) solvent by ultrasonication and mixing. Next, the solution was cast into membranes with a thickness of about 30 μm. The

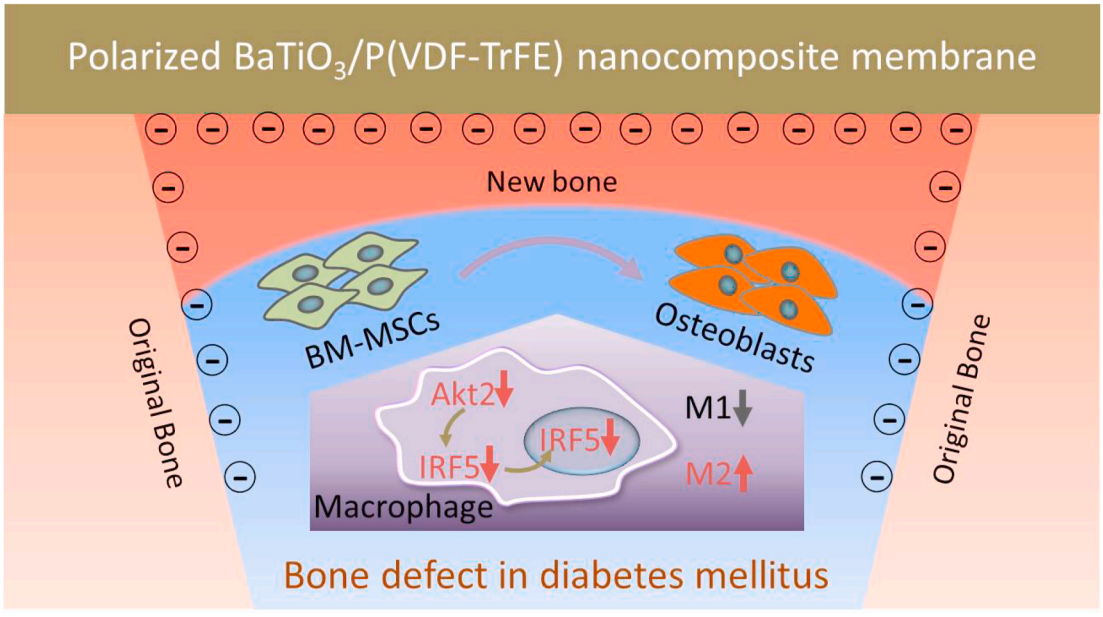

Scheme 1. Illustration of how electric microenvironment promotes osteogenesis in diabetes mellitus by modulating macrophage polarization. After corona poling treatment, the surface of the ferroelectric nanocomposite membrane displays induced charges. Within the electrical microenvironment, macrophages exhibit less M1 polarization and more M2 polarization. The polarized nanocomposite membranes downregulate AKT2-IRF5 signaling that induces macrophages to the M2 phenotype, which indicates a favorable osteo-immunomodulatory environment. Hence mimicking the endogeneous electrical microenvironment promotes osteogenic differentiation of BM-MSCs mediated by macrophages, thereby improving bone regeneration. The purple arrow denotes the osteogenesis of BM-MSCs. The grey arrows denote the suppressed M1 phenotype of macrophages. The red arrows denote the downregulated expression of AKT2 and IRF5, and improved M2 phenotype of macrophages.

membranes were then polarized using corona discharge with a DC field of 13 kV.

High-resolution transmission electron microscopy (HR-TEM, JEOL2011, JEOL, Tokyo, Japan) was performed to examine the coatings of modified BTO NPs. Field emission scanning electron microscopy (FE-SEM, S-4800, HITACHI, Tokyo, Japan) and X-ray diffraction spectroscopy (XRD, Rigaku D/max 2500 VB2t/PC, Rigaku Corporation, Tokyo, Japan) were used to characterize the surface morphology and crystallization. Atomic force microscopy (AFM, Auto-Probe CP, Park Scientific Instruments, San Francisco, USA) was performed to assess the surface roughness. To characterize the electrical properties, the polarization−-electric field (P−E) loop and piezoelectric coefficient (d33) were detected by a ferroelectric analyzer (TF1000, aixACCT Systems GmbH, Aachen, Germany) and a piezoelectric coefficient meter (ZJ-3AN, IACAS, Beijing, China) respectively.

2.2. Cell culture

Human monocytic THP-1 cells were maintained in glucose-free Roswell Park Memorial Institute medium (RPMI 1640, Hylcone, Utah, USA) supplemented with 10% (v/v) fetal bovine serum (FBS, Gibco, California, USA), 100 IU/ml penicillin-streptomycin and 5.5 mM D-glucose. THP-1 cells were differentiated into macrophages by treatment with 50 nM phorbol 12-myristate 13-acetate (PMA, P1585, Sigma, Missouri, USA) for 48h. High glucose cultured (HG) macrophages were incubated in glucose-free RPMI-1640 medium containing 10% (v/v) FBS, 100 IU/mL penicillin-streptomycin and 25 mM D-glucose to simulate uncontrolled sugar levels in diabetic patients. The high mannitol (HM) control macrophages were cultured in glucose-free RPMI-1640 medium containing 10% (v/v) FBS, 100 IU/mL penicillin-streptomycin 5.5 mM D-glucose and 19.5 D-manitol as an osmotic pressure control. After culturing for two days, macrophages (5×10^5 cells/ml) were subsequently analyzed. Macrophages were polarized into M1 or M2 phenotypes by treatment with 100 ng/ml LPS (L4391, Sigma, Missouri, USA) or 40 ng/ml IL-4 (204-IL-050, RD, Minnesota, USA) respectively. For RT-qPCR, ELSIA and Western blotting experiments, cells were treated with 100 ng/ml LPS as an inflammatory stimulator. To investigate the effects of AKT-IRF5 signaling on macrophage polarization following exposure to an electrical microenvironment, cells were co-cultured with LY294002 (S1737, Beyotime, Haimen, China) for 24h. Human BM-MSCs were obtained from Cyagen Bioscience Inc., and were cultured in Dulbecco's modified Eagle medium (S1737, Beyotime, Haimen, China) supplemented with 10% (v/v) FBS and 100 IU/mL penicillin-streptomycin. After two passages, BM-MSCs (5×10^4 cells/ml) were utilized in subsequent experiments. To investigate the effects of macrophages (cultured on various materials) on osteogenesis, BM-MSCs were cultured in media made up of collected macrophage culture supernatants and Human Mesenchymal Stem Cell Osteogenic Differentiation Medium (Cyagen Biosciences Inc., Guangzhou, China) containing 10% (v/v) FBS, 100 U/mL Penicillin-Streptomycin, 0.2 mM Ascorbate, 10 mM β-Glycerophosphate, 10^{-7} M Dexamethasone) at a ratio of 1:2. The normal culture medium without THP-1 cell supernatant was utilized as the control.

2.3. Cell spreading and imummocytochemistry

For assessment of cell spreading, the adherent cells on the various samples were fixed with 2.5% glutaraldehyde (w/v) and dehydrated through a graded ethanol series (30–100%) after 24h of culture. The cell morphology was examined by SEM. For iNOS staining, adherent macrophages were fixed in 4% (w/v) paraformaldehyde, and incubated with primary antibody against iNOS (ab15323, Abcam, Cambridgeshire, UK), followed by staining with FITC-conjugated goat anti-rabbit secondary antibody (ab150081, Abcam, Cambridgeshire, UK). Finally, the cell nuclei were labeled with 2-(4-amidinophenyl)-1H-indole-6-carboxamidine (DAPI, Roche, Basel, Switzerland). To evaluate osteogenic differentiation, immunocytochemical staining to detect osteogenic protein marker expression in BM-MSCs, including Runx-2, BMP-2 and COL1A, were performed for a period of 7 days, and images were captured under a confocal laser scanning microscope (Leica, Weztlar, Germany). Primary antibodies utilized include rabbit polyclonal anti-Runx-2 (ab23981, Abcam, Cambridgeshire, UK), anti-BMP-2 (ab6285, Abcam, Cambridgeshire, UK), and anti-COL I (ab6308, Abcam, Cambridgeshire, UK). Goat anti-rabbit (ab150081, Abcam, Cambridgeshire, UK) and goat anti-mouse antibodies (ab150115, Abcam, Cambridgeshire, UK) were utilized as secondary antibodies. The cell spreading area and integrated optical density (IOD) of iNOS immunostaining on the different materials were analyzed with the Image-pro Plus 6.0 software.

2.4. Flow cytometry analysis

Expression of M1 and M2 macrophage makers CD11c, CCR7 and CD206, respectively, were examined by flow cytometry. The cells were detached by scraping after 24h of culture. Cells were fixed in 4% (w/v) paraformaldehyde, blocked with 1% (w/v) BSA/PBS, and then incubated with antibodies against CD11c (301608, Biolegend, California, USA), CCR7 (353213, Biolegend, California, USA) and CD206 (321104, Biolegend, California, USA), respectively. The cells were then analyzed by a FACScalibur (BD Biosciences, New Jersey, America) instrument.

2.5. Microarray analysis

Total RNA from cells cultured on nanomembranes was extracted using the TRIzol reagent (Invitrogen, Carlsbad, Canada) and purified with Rneasy Mini Kit (Qiagen, Hilden, Germany) according to the manufacturer's instructions. Then Clariom D Array (Affymetrix GeneChip, Santa Clara, CA) was performed to construct the mRNA expression profiling. The raw data were normalized with Robust Multichip Analysis (RMA) algorithm and then analyzed by Affymetrix Transcriptome Analysis Console (TAC) Software (version4.0, Santa Clara, CA).

2.6. RT-qPCR and ELISA analysis

After culture for 1 day, macrophages on various samples were harvested by TRIzol (15596026, Invitrogen, California, USA). The extracted RNA was then reverse transcribed into cDNA using a reverse transcription system (RR037A, Toyobo, Osaka, Japan). The expression of genes, including IL-1β, IL-6, TNF-α, MIP-1α and MCP-1, was analyzed by an Applied Biosystems QuantStudio 3 thermocycler, utilizing the Quantitect Sybr Green Kit (Roche, Basel, Switzerland). The osteogenic gene marker expression of BM-MSCs, including Osterix, BMP-2 and BSP, were analyzed at the 7day timepoint using the same method. The primer sequences for the target genes are listed in Table S1.

To evaluate the cytokine secretion profile, the culture medium was collected after 1 day of culture. The secretion of IL-1β (ab214025, Abcam, Cambridgeshire, UK) and IL-6 (ab178013, Abcam, Cambridgeshire, UK) was assayed according to the manufacturer's instructions.

2.7. Western blotting

Cells were seeded on materials 1 day before the extraction of total cellular proteins, which were then subjected to SDS-PAGE and blotted onto nitorcellulose membranes according to standard protocols. After blocking with 5% (w/v) BSA, the membranes were incubated with primary antibodies against phosphorylated AKT2 (p-AKT2, 8599S, CST, Boston, USA), AKT2 (ab175354, Abcam, Cambridgeshire, UK), phosphorylated AKT (p-AKT, 4640, CST, Boston, USA), AKT (4685, CST, Boston, USA), IRF5 (20261S, CST, Boston, USA), HIF-1α (ab16066, Abcam, Cambridgeshire, UK), NF-κB (AF1234, Beyotime, Haimen, China) and β-actin (AF5003, Beyotime, Haimen, China). HRP-conjugated goat anti-mouse antibody (A0216, Beyotime, Haimen,

China) and HRP-conjugated goat anti-rabbit antibody (A0208, Haimen, China) were utilized as secondary antibodies. Western blot images were captured using the ChemiDoc Touch Imaging System (Bio-rad, California, USA).

2.8. Effects of macrophage-conditioned medium on the osteogenic differentiation of BM-MSCs

The Alkaline Phosphatase (ALP) activity of BM-MSCs was evaluated after 7 days of culture by an ALP activity assay kit (P0321, Beyotime, Haimen, China), according to the manufacturer's instructions. To assess ECM mineralization, the co-cultured cells were stained with 1% (w/v) Alizarin red S (A5533, Sigma, Missouri, USA) after 21 days of induction culture. For quantitative analysis, the alizarin red stain was dissolved in 10% (w/v) cetylpyridinium chloride (PHR1226, Sigma, Missouri, USA), prior to absorbance measurements at 620 nm.

2.9. In vivo immune response and evaluation of bone regeneration

2.9.1. Establishment of DM rat model and surgical procedures

All animal experiments were conducted in accordance with established ethical guidelines of the Animal Care and Use Committee of Peking University. Type 2 diabetes was established according to previously published protocol [8]. Briefly, six-week-old male Sprague-Dawley rats were fed with a high-fat diet (D12492, Research Diets, New Jersey, USA) for 4 weeks, and then injected with low-dose streptozotocin (30 mg/kg, S130, Sigma-Aldrich, Missouri, USA). Diabetes was considered to be successfully induced when fasting glucose levels were consistently over 11.1 mmol/L for 2 weeks. Subsequently, all animals were fed regular diets.

A total of twenty-four SD rats were utilized in the calvarial defect model as previously reported [19]. Firstly, the rats were anesthetized by intraperitoneal injection of 40 mg/kg pentobarbital sodium solution. Then a saline-cooled trephine drill was utilized to make two critical-sized full thickness bone defects (5 mm diameter) in rats at the center of each parietal bone. The right and the left defects were covered with polarized or unpolarized 5% (v/v) BTO NPs nanocomposite membranes, respectively. Whole calvarias were collected for evaluation at week 4 and week 8 post-implantation.

2.9.2. Flow cytometry and confocal fluorescence microscopy

To investigate the effects of the implanted polarized membranes on the immune response, flow cytometry and immunofluorescence staining were performed to assay macrophage polarization in interstitial fluids collected at the defect sites and on materials. The procedures were carried out as previously described in the above sections. The anti-CD11b (ab25533, Abcam, Cambridgeshire, UK), anti-CD11c (ab11029, Abcam, Cambridgeshire, UK), anti-CD206 (ab64693, Abcam, Cambridgeshire, UK), donkey anti-mouse (ab150105, Abcam, Cambridgeshire, UK) and goat anti-rabbit (ab150081, Abcam, Cambridgeshire, UK) antibodies were utilized in flow cytometry analysis. The anti-CD68 (ab955, Abcam, Cambridgeshire, UK), anti-iNOS (ab15323, Abcam, Cambridgeshire, UK), anti-CD206 (ab64693, Abcam, Cambridgeshire, UK), goat anti-mouse (ab150115, Abcam, Cambridgeshire, UK) and goat anti-rabbit antibodies (ab150081, Abcam, Cambridgeshire, UK) were utilized in immunofluorescence staining.

2.9.3. Microcomputed tomography (μ-CT), immunohistochemistry and histology analysis

The specimens were examined with μ-CT as previously described. A modified Feldkamp algorithm was performed to reconstruct files, which was created utilizing a microtomographic analysis software (Tomo NT, Skyscan, Kontich, Belgium). The quantitative analysis of bone volume to total volume (BV/TV), bone mineral density (BMD), trabecular-number and trabecular-thickness was performed on the defect region.

For immunohistochemistry and histological analyses, tissue processing and sectioning after the removal of nanomembranes were performed, as described by our previous study [19]. Briefly, paraffin-embedded tissue samples were sectioned at 5 μm thickness after dehydration in a graded ethanol series (70–100%). Then mouse polyclonal anti-IL-6 (ab9324, Abcam, Cambridgeshire, UK) and HRP-conjugated goat anti-mouse antibodies (ab205719, Abcam, Cambridgeshire, UK) were utilized for immunohistochemistry analysis. Based on the manufacturer's instruction, H&E staining and Masson's trichrome staining were carried out separately for histological observations, and digital images were captured under polarized light microscopy (CX21, Olympus, Tokyo, Japan).

2.10. Statistical analysis

All results were expressed as means ± SD. Statistical comparisons between groups were analyzed using one-way analysis of variance (ANOVA). A value of $p < 0.05$ was considered statistically significant.

3. Results and discussion

3.1. The design and fabrication of biomimetic electroactive nanocomposite membranes

To mimic the electrical microenvironment of native bone ECM, polarized BTO/P(VDF-TrFE) nanocomposite membranes were fabricated by utilizing a straightforward solution-casting method (Fig. 1a) according to our previous study [19]. Polydopamine coating of BTO NP (Fig. S1a) was used to improve the interface compatibility with P(VDF-TrFE) matrix, which gives rise to a more uniform distribution of BTO NPs throughout the films (Fig. 1b). Various analyses such as X-Ray diffraction (XRD) spectra (Fig. S1b), ferroelectric behavior with hysteresis loops (Fig. 1c) and atomic force microscope (AFM) analysis (Figs. 1d and S1d) were performed to confirm that the fabricated BTO/P(VDF-TrFE) membranes were similar to that of our previous study [19]. This nanocomposite membrane has a surface potential that was similar to physiological values, which has been validated by our previous research [19]. The electrical stability test results under simulated physiological conditions (Fig. S1c) showed that the continuous stable piezoelectric coefficient (about 8.19 pC/N) of the nanocomposite membrane is consistent with that of native bone [20]. These results thus imply that our nanocomposite membrane might have the ability to provide a electrical microenvironment to enhance osteogenesis under hyperglycemic conditions.

3.2. Electrical microenvironment attenuates M1 macrophage polarization under hyperglycemic conditions

Hyperglycemia is considered a key hallmark in diabetic pathology, and inflammation is an essential part of the pathological process [5]. Macrophages are key innate immune cells which coordinate inflammatory and healing processes via a delicate balance between two distinct polarization states: classically-activated M1 macrophages and alternatively-activated M2 macrophages. We first established a model to evaluate the influence of high glucose (HG) conditions on macrophage polarization. Cell morphology has been reported to modulate the polarized state of macrophages [21]. Microscopy images showed that HG-cultured cells displayed the largest cell spreading area and adopted a fried egg-like shape with much filopodia that presented a typical M1-like appearance, unlike the more typical round shape that indicates a resting non-activated macrophage (M0), as observed in the normal glucose (NG) and high mannitol (HM) groups (Figs. S2a and b). The expression of specific markers such as iNOS by M1 macrophages were assessed by immunocytochemistry. iNOS expression was obviously enhanced in the HG group while there were no discernible differences between the NG and HM groups (Figs. S2c and d). Furthermore, population polarization trends were evaluated by flow cytometry analysis for M1 (CD11c) and

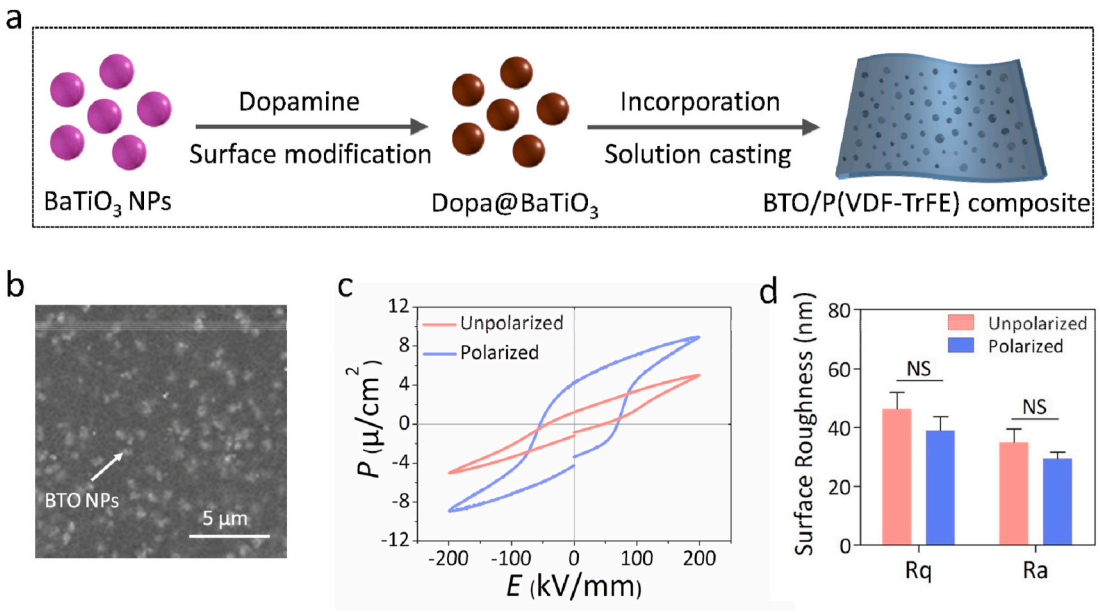

Fig. 1. Fabrication and characterization of BTO/P(VDF-TrFE) composite membranes. (a) Schematic representation of BTO/P(VDF-TrFE) nanocomposite membrane fabrication. **(b)** Representative SEM images of nanocomposite membranes. The white arrow denotes the BTO NPs. **(c)** The hysteresis loops of unpolarized and polarized BTO/P(VDF-TrFE) membranes. **(d)** Surface roughness analysis of unpolarized and polarized membranes (n = 3).

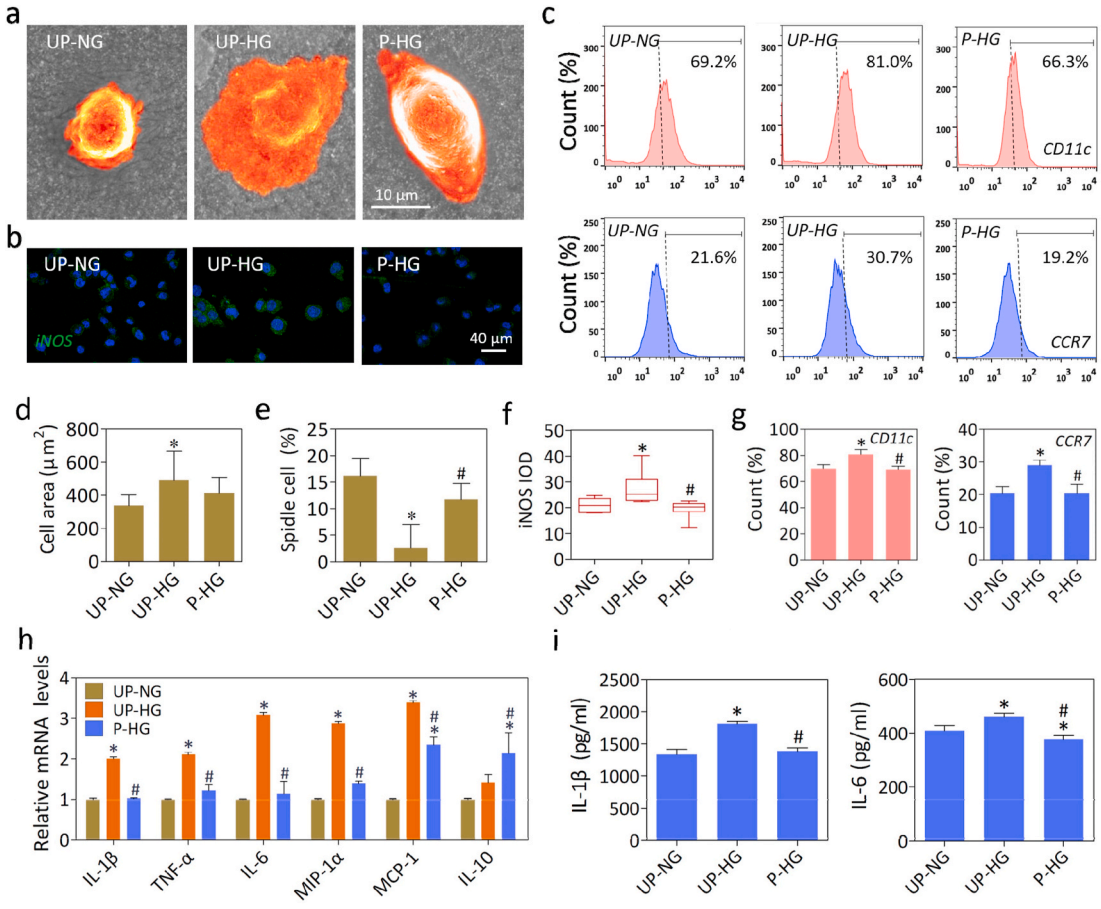

Fig. 2. Electrical microenvironment regulates phenotypic changes in high glucose induced macrophages. (a, d and e) Representative SEM images and quantitative analysis of cell area and spindle cell ratio of macrophages cultured with different conditions. **(b, f)** Representative immunofluorescence images and quantitative analysis of iNOS (green) and cell nuclei (DAPI, blue) in macrophages cultured for 24h. **(c, g)** Flow cytometry and quantitative analysis of cell surface markers CD11c and CCR7 under different conditions. **(h, i)** The mRNA expression levels and secretion of representative cytokine genes in LPS-stimulated macrophage cultured on various different materials. *denotes significantly different from the UP-NG group, # denotes significantly different from the UP-HG group (n ≥ 3).

M2 (CD206) markers. M1 polarization was markedly up-regulated in the HG group that is consistent with iNOS expression, while no significant differences were observed in M2 polarization between groups (Fig. S2e). Macrophages contribute to tissue repair by secretion of various cytokines [22]. RT-qPCR analysis showed that the expression of pro-inflammatory genes such as TNF-α, IL-6, MIP-1α and MCP-1 were significantly increased in the HG versus control group, while there were no significant differences in response to hyperosmotic conditions (Fig. S2f). Similarly, an increase of IL-6 and IL-8 secretion was observed in LPS-stimulated U937 monocytes exposed to high glucose [23]. These results thus indicate that high glucose conditions promote macrophage polarization to the M1 phenotype, which is known to impede wound healing [24].

The immunomodulatory effects of polarized nanocomposite membranes were further investigated in the hyperglycemic macrophage model. SEM imaging showed that macrophages presented a fried egg-like shape with much filopodia on unpolarized membranes cultured with high glucose concentration (UP-HG), while most cells displayed a typical round appearance on the unpolarized membranes cultured with normal glucose concentration (UP-NG) or polarized membranes cultured with high glucose concentration (P-HG) (Fig. 2a and Fig. S3a). Additionally, some cells in the UP-NG and P-HG groups adopted a spindle-like shape. Meanwhile, the cell spreading area and spindle cell ratio analysis showed that cells in the UP-HG group exhibited M1-like shape and large spreading area, while some cells in the P-HG group displayed a spindle-like shape that is considered typical M2-like morphology (Fig. 2d and e) [21]. Moreover, as shown in Fig. S3b, it was obvious that the area of focal adhesion (FA) in the UP-HG and P-HG groups were greater than that of UP-NG group. The FA of the UP-HG groups exhibited a dense ring-like pattern, whereas the polarized nanomembranes were mostly distributed in the unilateral region. Therefore, the differences in FA formation and morphology clearly indicated that macrophages would be more prone to M1 type activation in the UP-HG group, as compared to the UP-NG and P-HG groups.

Next, we evaluated effects on macrophage polarization under different conditions. The immunofluorescence staining data and quantitative analysis showed that polarized membranes significantly attenuated iNOS expression (Fig. 2b, f). With regards to M1 macrophage surface markers, an obvious increase in CD11c and CCR7 expression were observed in macrophages exposed to high glucose concentration (UP-HG), as compared to macrophages exposed to normal glucose concentration (UP-NG) or high glucose concentration with an electrical microenvironment (P-HG) (Fig. 2c, g). Moreover, the ratio of M2 macrophages (CD206+) was increased on the polarized nanomembranes (P-HG), as compared to the UP-HG group (Fig. S4). These results suggest that the biomimetic electrical microenvironment could attenuate high glucose induced M1 macrophage polarization and promote M2 macrophage polarization.

To further evaluate the cytokine production profile, RT-qPCR and ELISA assays were performed. There were significantly up-regulated expression of the pro-inflammatory cytokine gene markers including IL-1β, IL-6, TNF-α, MIP-1α and MCP-1 in the UP-HG group upon LPS stimulation (Fig. 2h). Meanwhile, the expression levels of pro-inflammatory gene markers were significantly down-regulated, while IL-10 expression was obviously up-regulated on the polarized nanomembranes (P-HG), as compared to unpolarized membranes (UP-HG). Moreover, the secretion of IL-1β and IL-6 demonstrates that the electrical microenvironment could mitigate the stimulatory effects of high glucose in promoting pro-inflammatory cytokine secretion by macrophages (Fig. 2i). All these results thus imply that the electrical microenvironment could neutralize the inductive effects of high glucose in stimulating pro-inflammatory cytokine production by macrophages upon LPS treatment.

Our data on cell spreading, M1 marker expression, pro-inflammatory gene expression and cytokine production showed that the pro-inflammatory M1 phenotype of macrophages was enhanced by high glucose, but these pro-inflammatory effects were obviously attenuated on polarized nanocomposite membranes. Hence, it can be inferred that the biomimetic electrical microenvironment could restore the balance of macrophage function under hyperglycemic conditions, which resulted in a favorable osteo-immunomodulatory effect.

3.3. Electrical microenvironment promotes osteogenic differentiation by modulating macrophage polarization in vitro

The osteogenic differentiation of BM-MSCs cultured with macrophage conditioned medium was further evaluated by analyzing osteogenic gene and protein expression, ALP activity and mineral deposition (Fig. 3). After incubation for 7 days, expression levels of the osteogenic gene markers BMP-2 and BSP were significantly downregulated in cells cultured with UP-HG versus UP-NG conditioned medium, while the expression levels of Osterix, BMP-2 and BSP were significantly upregulated in cells cultured with P-HG versus UP-HG conditioned medium (Fig. 3a). The ALP activity assay showed a similar trend with the UP-HG group exhibiting the lowest ALP activity level. By contrast, P-HG displayed the highest ALP activity level (Fig. 3b). Moreover, Alizarin Red staining and quantitative analysis demonstrated that only small mineralized nodules were observed in the UP-HG group, but the negative effect of high glucose levels on osteogenic differentiation was counteracted in the P-HG group (Fig. 3c). Additionally, it is apparent in the immunostaining images that the protein expression levels of Runx-2, BMP-2 and COL1 were decreased in the UP-HG versus UP-NG group, but were recovered in the P-HG group (Fig. 3d, e, f and g). All these results thus suggest that the electric microenvironment displays excellent macrophage mediated osteoinductivity under hyperglycemic conditions. This favorable effect could be attributed to macrophages exhibiting reduced expression of IL-6, a typical pro-inflammatory cytokine, which is closely associated with bone resorption in diabetic patients [25].

3.4. Restored electrical microenvironment regulates macrophage polarization and improves bone regeneration in diabetes mellitus rats

We next investigated whether the electrical microenvironment can exert positive effects on bone defect repair in a diabetic rat model. Polarized nanocomposite membranes were implanted to cover freshly-formed 5-mm critical-sized calvarial defects in rats with type 2 diabetes mellitus. As shown by the flow cytometry analysis data (Fig. 4a), the polarized nanocomposite membrane group displayed lower proportions of M1 macrophages (CD11b+CD11c+) at day 4 and significantly higher M2 polarization (CD11b+CD206+) at day 14, as compared to unpolarized nanocomposite membranes. Moreover, similar trends were also observed in iNOS and CD206 expression by adherent macrophages in the immunocytochemistry data (Fig. 4c). These results suggest that polarized membranes inhibited M1 polarization at early inflammatory stages, but enhanced M2 polarization during the wound healing stage [26–28]. In addition, markedly higher expression of the M1 inflammatory cytokine IL-6 was also demonstrated by immunohistochemical staining. After 1 week, we observed markedly higher expression of IL-6 on the unpolarized versus polarized nanocomposite membrane group (Fig. 4b), which is consistent with the results *in vitro*.

Subsequently, the effects on the M2/M1 ratio mediated by electrical microenvironment on bone regeneration were investigated in the presence of diabetes. As evidenced by micro-CT images, polarized group promoted more new bone formation than unpolarized group at both week 4 and week 8 post-surgery. Especially, the defect site was almost completely filled with newly regenerated bone in the polarized group, whereas only a thin layer of newly regenerated bone was observed in the unpolarized group after 8 weeks of implantation (Fig. 4d). As expected, the quantitative analysis results showed that the polarized nanocomposite membranes led to a substantial increase in BV/TV, BMD and trabecular number, and a slight increase in trabecular thickness at week

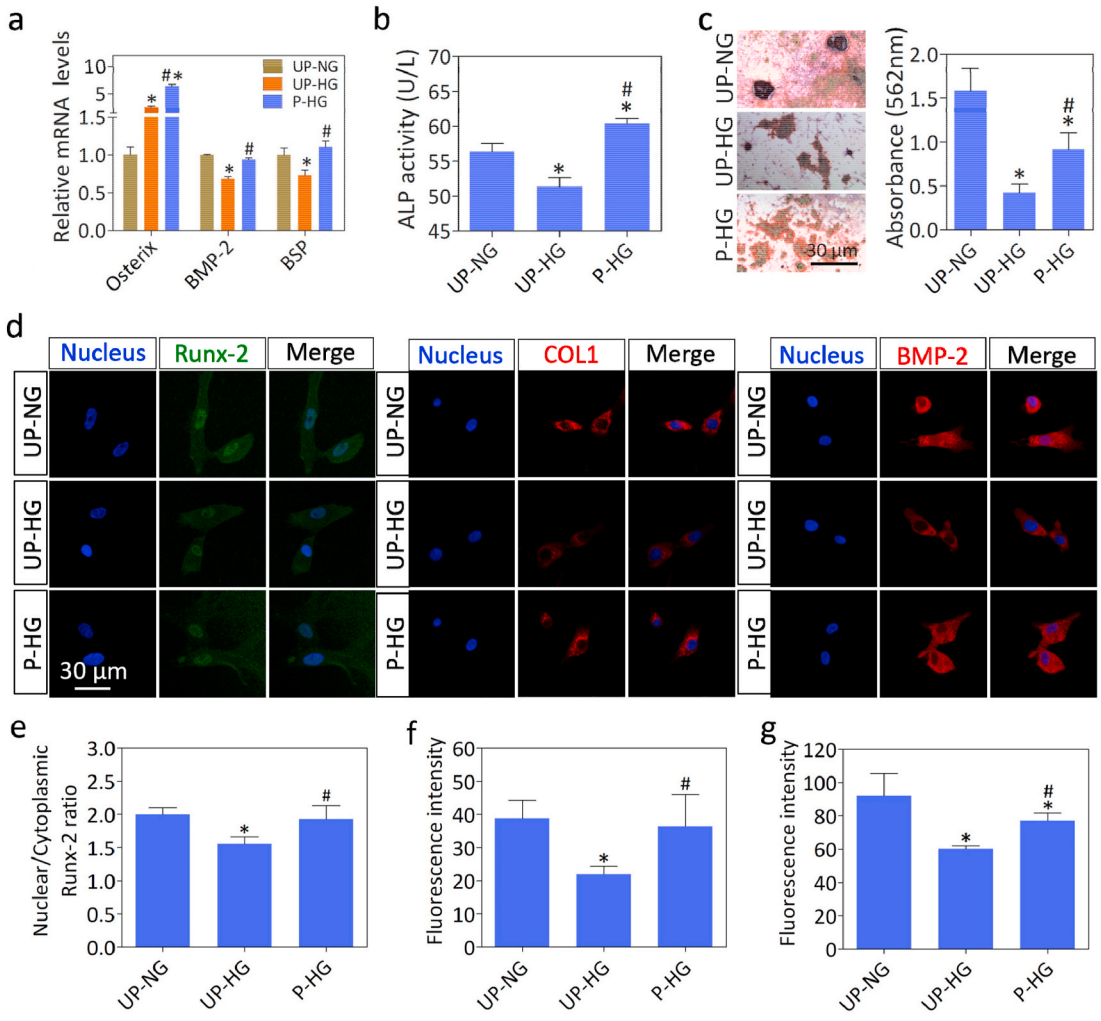

Fig. 3. Macrophage heterogeneity affects behavior of BM-MSCs cultured *in vitro*. **(a)** The mRNA expression levels of osteogenic gene markers in BM-MSCs cultured in conditioned medium for 7 days. **(b)** ALP activity assay of BM-MSCs at one week. **(c)** Representative images and quantitative analysis of Alizarin Red S staining of BM-MSCs cultured for 21 days. **(d, e, f and g)** Representative immunostaining images and quantitative analysis of RUNX-2 (green), BMP-2 (red), COLI (red) and cell nuclei (DAPI, blue) in BM-MSCs cultured for 7 days. * denotes significantly different from the UP-NG group, # denotes significantly different from the UP-HG group ($n \geq 3$).

8 post-implantation. (Fig. 4f and Fig. S5). Furthermore, as evidenced by H&E and Masson's trichrome staining, mature osteoid tissue was present and the skull was mostly reconstructed in polarized membranes group, while a large amount of fibrous connective tissue still occupies the center of the defect in unpolarized membranes group after 8 weeks of implantation (Fig. 4e). These results thus indicate that the polarized BTO/P(VDF-TrFE) nanocomposite membrane is a promising immunomodulatory biomaterial that can regulate local inflammation to provide a favorable osteo-immunomodulatory microenvironment, thereby accelerating bone regeneration under DM condition. Surface properties of implanted biomaterials have long been considered as key parameter that could guide macrophage polarization and improve bone healing efficiency under diabetic conditions [29–31]. Therefore, our results identified electrical properties as a new crucial parameter of biomaterials that can modulate macrophage polarization and bone regeneration.

3.5. The AKT2-IRF5 signaling axis was downregulated within macrophages under hyperglycemic conditions in an electrical microenvironment

Having established that the electric microenvironment plays a pivotal role in regulating macrophage fate, we next investigated how the polarized nanocomposite membranes influence macrophage polarization. To elucidate the underlying mechanisms of electrical microenvironment mediated immuno-regulatory osteogenesis, gene microarrays were performed to analyze temporal mRNA expression patterns on different membranes. A large number of differentially-expressed genes were identified in the various groups (Fig. S6a). The hierarchical cluster analysis of differentially overlapping gene among these groups showed that macrophages on polarized nanomembranes exhibited a gene expression profile that was more similar to the control group, as compared to unpolarized membranes, which indicated that the electrical microenvironment could mitigate the adverse effects of high glucose on macrophage gene expression (Fig. S6b). Subsequently, pathway enrichment analysis indicated that the PI3K-AKT pathway was correlated with suppressed expression of M1 phenotypic markers (Fig. 5a). Furthermore, a growing body of scientific literature has demonstrated that AKT plays a key role in regulating macrophage heterogeneous polarization [32,33]. AKT2, IRF5 and STAT1 are the master regulators of M1 activation, while AKT1 is the key regulator of M2 activation [34,35]. In this study, significantly different AKT2 expressions at the mRNA and protein levels were observed in the different groups (Fig. 5b, c and Fig. S7a). Phosphorylation is known to be

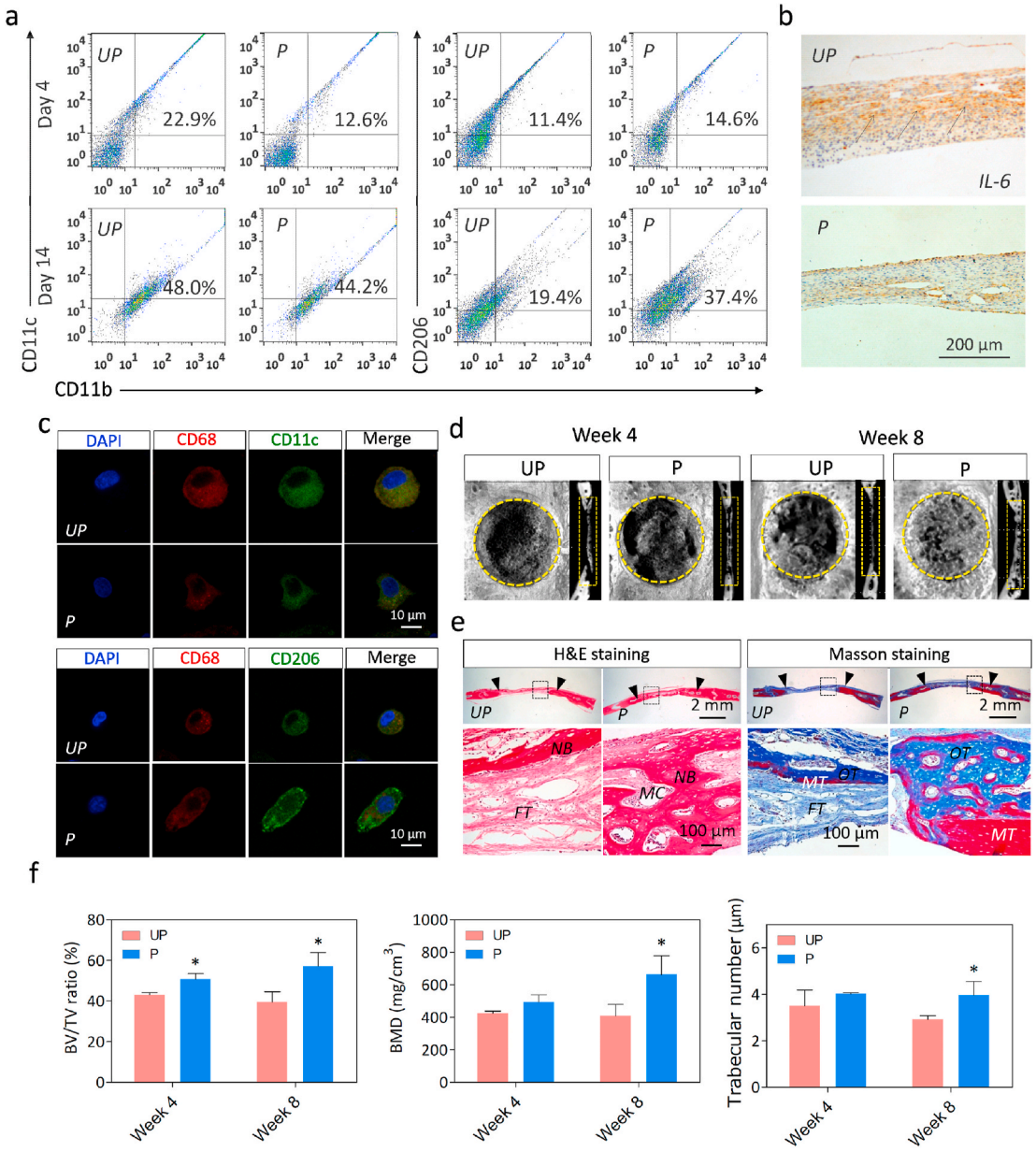

Fig. 4. Restored Electrical microenvironment regulates immune function and bone defect repair in diabetic rats. (a) Flow cytometry analysis of macrophage phenotype at 4d and 14d. **(b)** Immunohistochemical imaging of IL-6 expression in histological sections at week 1 post-implantation. The black arrows denote IL-6 positive regions. **(c)** Representative immunostaining images of M1 (CD68+iNOS+) and M2 ($CD68^{+}CD206+$) at day 14. **(d)** Representative micro-CT images of critical-sized rat calvarial full-thickness defects at week 4 and week 8 post-implantation. The yellow circles and rectangles denote the defect sites. **(e)** HE and Masson's trichrome staining of histological sections at week 8 post-implantation. The black arrows denote the line between nascent bone and host bone. (NB, nascent bone; FT, fibrous tissue; MC, medullary cavity; OT, osteoid tissue; MT, mineralized tissue). **(f)** Quantitative analysis of BV/TV, BMD and trabecular number. *denotes significantly different from the UP group (n = 3).

indispensable for AKT function in the regulation of biological processes. Downregulation of phosphorylated AKT2 with specific agents was demonstrated to attenuate M1 polarization (Fig. 5f, g and Fig. S7b). These results thus confirmed that phosphorylated AKT2 and AKT2 play crucial roles in electrical microenvironment-mediated macrophage polarization and induced bone regeneration.

Furthermore, IRF5, a key transcriptional factor, has been reported to regulate glycolysis and human M1 macrophage activation via AKT2 activation [36]. In this study, we found that IRF5 and HIF-1α expression were significantly upregulated in macrophages on unpolarized membranes exposed to high glucose conditions, whereas there was significantly downregulated expression on polarized membranes (Fig. 5b, d and Fig. S7c). Moreover, a marked reduction of IRF5 expression was accompanied by inhibition of AKT2 phosphorylation (Fig. 5e and Fig. S7d). Additionally, the expression of HIF-1α, a master regulator of glycolysis, displayed similar trends [37]. These results thus demonstrated that AKT2 and IRF5 could reciprocally regulate each other to control macrophage cell fate. Taken together, the electric microenvironment could sequentially modulate AKT2-IRF5/HIF-1α signaling to effect macrophage polarization, glycolysis, and osteogenic differentiation of BM-MSCs, thereby improving bone regeneration under DM conditions.

4. Conclusion

In conclusion, we demonstrate that the polarized ferroelectric

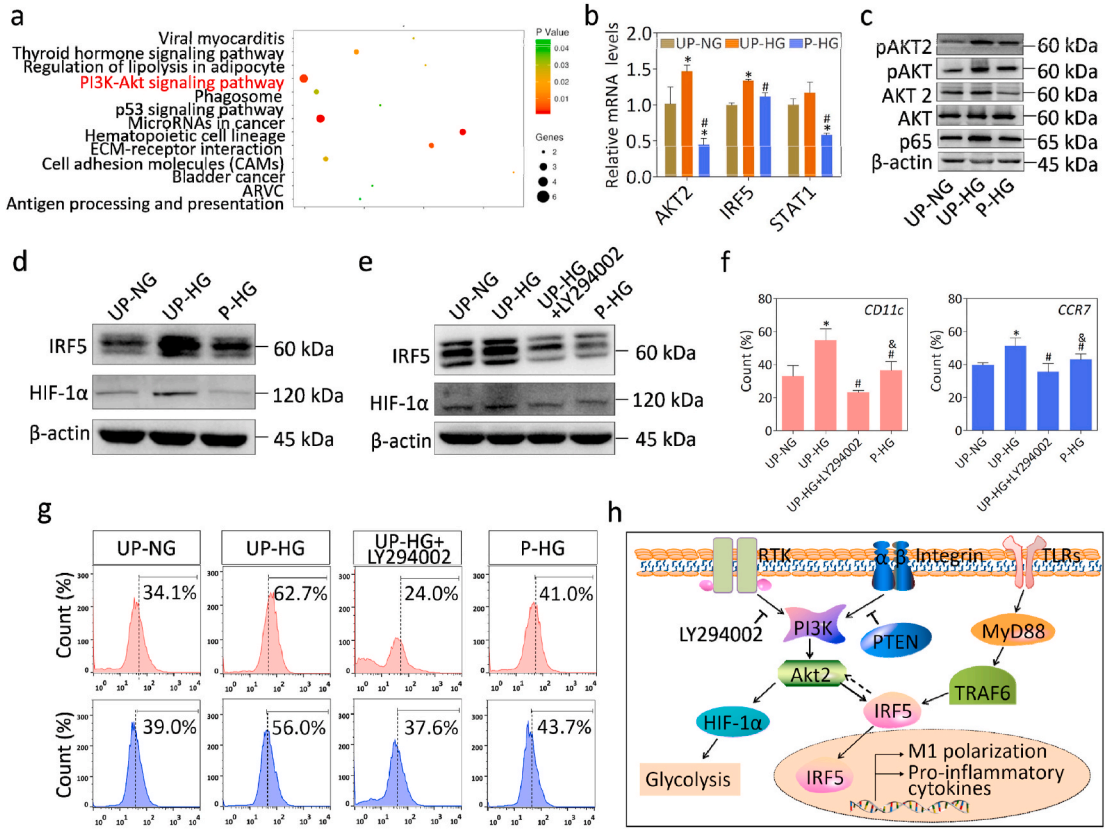

Fig. 5. Electrical microenvironment mediates the phenotypic changes of macrophages by the AKT2-IRF5 signaling pathway. (a) Pathway Enrichment analysis of normalized gene expression data in each group by microarray analysis. **(b)** The mRNA expression levels of pathway genes in each group. **(c)** The AKT2 and phosphorylatd AKT2 were activated under high glucose conditions and inhibited in an electrical microenviroenvirnment. **(d, e)** The expression of IRF5 and HIF-1α in cells treated with or without AKT inhibitor. **(f, g)** Flow cytometry analysis of cell surface markers CD11c and CCR7 under different conditions. **(h)** The schematic representation of molecular signaling events that mediates electrical microenvironment-induced macrophage polarization. *denotes significantly different from the UP-NG group, #denotes significantly different from the UP-HG group (n = 3).

nanocomposite membranes with conducive electrical properties can modulate macrophage polarization and osteogenic differentiation of BM-MSCs, thereby enhancing bone regeneration by mimicking the endogeneous electrical microenvironment of native bone tissues. Our data conclusively showed that the electrical microenvironment induced by the polarized ferroelectric nanocomposite membranes improved the osteo-immunmodulatory microenvironment and promoted osteogenesis via the AKT2-IRF5 signaling pathway. Our findings on electrical microenvironment-mediated osteoimmunomodulation offer a promising and efficient strategy for facilitating bone regeneration under DM conditions. This study provides the basis for further research and development of electroactive biomaterials, which might have important clinical significance for achieving a favorable immunomodulatory microenvironment for tissue regeneration and treatment of diseases linked with inflammation, such as arthritis and atherosclerosis.

CRediT authorship contribution statement

Xiaohan Dai: Investigation, Formal analysis, Methodology, Software, Validation, Funding acquisition, Writing - original draft. **Boon Chin Heng:** Formal analysis, Methodology, Funding acquisition, Writing - original draft. **Yunyang Bai:** Investigation, Methodology, Validation, Funding acquisition. **Fuping You:** Methodology, Writing - review & editing. **Xiaowen Sun:** Investigation, Formal analysis, Software, Validation. **Yiping Li:** Methodology, Writing - review & editing. **Zhangui Tang:** Methodology, Writing - review & editing. **Mingming Xu:** Conceptualization, Supervision, Writing - review & editing. **Xuehui Zhang:** Conceptualization, Funding acquisition, Supervision, Writing - review & editing. **Xuliang Deng:** Conceptualization, Funding acquisition, Project administration, Writing - review & editing.

Declaration of competing interest

The authors declare that they have no competing interests.

Acknowledgments

This work was supported by the National Key R&D Program of China (2018YFC1105303/04), National Natural Science Foundation of China (Nos. 51772006, 31670993, 51973004, 81991505, 82022016), Beijing Municipal Science & Technology Commission Projects (Z181100002018001), Peking University Medicine Fund (Nos. PKU2020LCXQ009, BMU2020PYB029), Natural Science Foundation of Hunan Province (2019JJ50779) and Health and Family Planning Commission of Hunan Province (20180246).

Appendix A. Supplementary data

Supplementary data to this article can be found online at https://doi.org/10.1016/j.bioactmat.2020.12.020.

References

[1] T. Szkudelski, K. Szkudelska, Resveratrol and diabetes: from animal to human studies, BBA-Biomembranes 1852 (2015) 1145–1154.
[2] D.R. Whiting, L. Guariguata, C. Weil, J. Shaw, IDF diabetes atlas: global estimates of the prevalence of diabetes for 2011 and 2030, Diabetes Res. Clin. Pract. 94 (2011) 311–321.

[3] P.K. Moy, D. Medina, V. Shetty, T.L. Aghaloo, Dental implant failure rates and associated risk factors, Int. J. Oral Maxillofac. Implants 20 (2005) 569–577.
[4] D. Merlotti, L. Gennari, F. Dotta, D. Lauro, R. Nuti, Mechanisms of impaired bone strength in type 1 and 2 diabetes, Nutr Metab Cardiovas 20 (2010) 683–690.
[5] M. Miao, Y. Niu, T. Xie, B. Yuan, C. Qing, S. Lu, Diabetes-impaired wound healing and altered macrophage activation: a possible pathophysiologic correlation, Wound Repair Regen. 20 (2012) 203–213.
[6] N. Esser, S. Legrand-Poels, J. Piette, A.J. Scheen, N. Paquot, Inflammation as a link between obesity, metabolic syndrome and type 2 diabetes, Diabetes Res. Clin. Pract. 105 (2014) 141–150.
[7] G. Colleluori, L. Aguirre, R. Dorin, D. Robbins, D. Blevins, Y. Barnouin, R. Chen, C. Qualls, D.T. Villareal, R. Armamento-Villareal, Hypogonadal men with type 2 diabetes mellitus have smaller bone size and lower bone turnover, Bone 99 (2017) 14–19.
[8] Z. Hu, C. Ma, X. Rong, S. Zou, X. Liu, Immunomodulatory ECM-like microspheres for accelerated bone regeneration in diabetes mellitus, ACS Appl. Mater. Interfaces 10 (2018) 2377–2390.
[9] P.C. Dias, P. Limirio, C.R.B. Linhares, M.L. Bergamini, F.S. Rocha, R.B. Morais, A.P. C. Balbi, K.R.N. Hiraki, P. Dechichi, Hyperbaric Oxygen therapy effects on bone regeneration in Type 1 diabetes mellitus in rats, Connect. Tissue Res. 59 (2018) 574–580.
[10] C. Wallner, S. Abraham, J.M. Wagner, K. Harati, B. Ismer, L. Kessler, H. Zollner, M. Lehnhardt, B. Behr, Local application of isogenic adipose-derived stem cells restores bone healing capacity in a type 2 diabetes model, Stem cells translational medicine 5 (2016) 836–844.
[11] C.I. Cheng, P.H. Chen, Y.C. Lin, Y.H. Kao, High glucose activates Raw264.7 macrophages through RhoA kinase-mediated signaling pathway, Cell. Signal. 27 (2015) 283–292.
[12] I. Torres-Castro, U.D. Arroyo-Camarena, C.P. Martinez-Reyes, A.Y. Gomez-Arauz, Y. Duenas-Andrade, J. Hernandez-Ruiz, Y.L. Bejar, V. Zaga-Clavellina, J. Morales-Montor, L.I. Terrazas, J. Kzhyshkowska, G. Escobedo, Human monocytes and macrophages undergo M1-type inflammatory polarization in response to high levels of glucose, Immunol. Lett. 176 (2016) 81–89.
[13] T.A. Wynn, A. Chawla, J.W. Pollard, Macrophage biology in development, homeostasis and disease, Nature 496 (2013) 445–455.
[14] P.J. Murray, J.E. Allen, S.K. Biswas, E.A. Fisher, D.W. Gilroy, S. Goerdt, S. Gordon, J.A. Hamilton, L.B. Ivashkiv, T. Lawrence, M. Locati, A. Mantovani, F.O. Martinez, J.L. Mege, D.M. Mosser, G. Natoli, J.P. Saeij, J.L. Schultze, K.A. Shirey, A. Sica, J. Suttles, I. Udalova, J.A. van Ginderachter, S.N. Vogel, T.A. Wynn, Macrophage activation and polarization: nomenclature and experimental guidelines, Immunity 41 (2014) 14–20.
[15] C.A. Bassett, R.J. Pawluk, R.O. Becker, Effects of electric currents on bone in vivo, Nature 204 (1964) 652–654.
[16] R.D. Saunders, C.D. McCaig, Developmental effects of physiologically weak electric fields and heat: an overview, Bioelectromagneti. Suppl 7 (2005) S127–S132.
[17] J.I. Hoare, A.M. Rajnicek, C.D. McCaig, R.N. Barker, H.M. Wilson, Electric fields are novel determinants of human macrophage functions, J. Leukoc. Biol. 99 (2016) 1141–1151.
[18] Z. Akan, B. Aksu, A. Tulunay, S. Bilsel, A. Inhan-Garip, Extremely low-frequency electromagnetic fields affect the immune response of monocyte-derived macrophages to pathogens, Bioelectromagnetics 31 (2010) 603–612.
[19] X. Zhang, C. Zhang, Y. Lin, P. Hu, Y. Shen, K. Wang, S. Meng, Y. Chai, X. Dai, X. Liu, Y. Liu, X. Mo, C. Cao, S. Li, X. Deng, L. Chen, Nanocomposite membranes enhance bone regeneration through restoring physiological electric microenvironment, ACS Nano 10 (2016) 7279–7286.
[20] C. Halperin, S. Mutchnik, A. Agronin, M. Molotskii, P. Urenski, M. Salai, G. Rosenman, Piezoelectric effect in human bones studied in nanometer scale, Nano Lett. 4 (2004) 1253–1256.
[21] F.Y. McWhorter, T. Wang, P. Nguyen, T. Chung, W.F. Liu, Modulation of macrophage phenotype by cell shape, PNAS 110 (2013) 17253–17258.
[22] G. Arango Duque, A. Descoteaux, Macrophage cytokines: involvement in immunity and infectious diseases, Front. Immunol. 5 (2014) 491.
[23] J. Haidet, V. Cifarelli, M. Trucco, P. Luppi, C-peptide reduces pro-inflammatory cytokine secretion in LPS-stimulated U937 monocytes in condition of hyperglycemia, Inflamm. Res. 61 (2012) 27–35.
[24] A.E. Boniakowski, A.S. Kimball, B.N. Jacobs, S.L. Kunkel, K.A. Gallagher, Macrophage-mediated inflammation in normal and diabetic wound healing, J. Immunol. 199 (2017) 17–24.
[25] K. Yokota, K. Sato, T. Miyazaki, H. Kitaura, H. Kayama, F. Miyoshi, Y. Araki, Y. Akiyama, K. Takeda, T. Mimura, Combination of tumor necrosis factor alpha and interleukin-6 induces mouse osteoclast-like cells with bone resorption activity both in vitro and in vivo, Arthritis Rheum. 66 (2014) 121–129.
[26] R. Sridharan, A.R. Cameron, D.J. Kelly, C.J. Kearney, F.J. O'Brien, Biomaterial based modulation of macrophage polarization: a review and suggested design principles, Mater. Today 18 (2015) 313–325.
[27] K. Deonarine, M.C. Panelli, M.E. Stashower, P. Jin, K. Smith, H.B. Slade, C. Norwood, E. Wang, F.M. Marincola, D.F. Stroncek, Gene expression profiling of cutaneous wound healing, J. Transl. Med. 5 (2007) 11.
[28] K.A. Kigerl, J.C. Gensel, D.P. Ankeny, J.K. Alexander, D.J. Donnelly, P.G. Popovich, Identification of two distinct macrophage subsets with divergent effects causing either neurotoxicity or regeneration in the injured mouse spinal cord, J. Neurosci. 29 (2009) 13435–13444.
[29] R.S.B. Lee, S.M. Hamlet, S. Ivanovski, The influence of titanium surface characteristics on macrophage phenotype polarization during osseous healing in type I diabetic rats: a pilot study, Clin. Oral Implants Res. 28 (2017) e159–e168.
[30] Z. Hu, X. Wang, W. Xia, Z. Wang, P. Zhang, L. Xia, K. Lin, M. Zhu, Nano-structure designing promotion osseointegration of hydroxyapatite coated Ti-6Al-4V alloy implants in diabetic model, J. Biomed. Nanotechnol. 15 (2019) 1701–1713.
[31] N. Tan, X. Liu, Y. Cai, S. Zhang, B. Jian, Y. Zhou, X. Xu, S. Ren, H. Wei, Y. Song, The influence of direct laser metal sintering implants on the early stages of osseointegration in diabetic mini-pigs, Int. J. Nanomed. 12 (2017) 5433–5442.
[32] M.F. Linton, J.J. Moslehi, V.R. Babaev, Akt signaling in macrophage polarization, survival, and atherosclerosis, Int. J. Mol. Sci. 20 (2019).
[33] E. Vergadi, E. Ieronymaki, K. Lyroni, K. Vaporidi, C. Tsatsanis, Akt signaling pathway in macrophage activation and M1/M2 polarization, J. Immunol. 198 (2017) 1006–1014.
[34] A. Arranz, C. Doxaki, E. Vergadi, Y. Martinez de la Torre, K. Vaporidi, E. D. Lagoudaki, E. Ieronymaki, A. Androulidaki, M. Venihaki, A.N. Margioris, E. N. Stathopoulos, P.N. Tsichlis, C. Tsatsanis, Akt1 and Akt2 protein kinases differentially contribute to macrophage polarization, PNAS 109 (2012) 9517–9522.
[35] T. Krausgruber, K. Blazek, T. Smallie, S. Alzabin, H. Lockstone, N. Sahgal, T. Hussell, M. Feldmann, I.A. Udalova, IRF5 promotes inflammatory macrophage polarization and TH1-TH17 responses, Nat. Immunol. 212 (2011) 231–238.
[36] M. Hedl, J. Yan, C. Abraham, IRF5 and IRF5 disease-risk variants increase glycolysis and human M1 macrophage polarization by regulating proximal signaling and Akt2 activation, Cell Rep. 16 (2016) 2442–2455.
[37] H. Semba, N. Takeda, T. Isagawa, Y. Sugiura, K. Honda, M. Wake, H. Miyazawa, Y. Yamaguchi, M. Miura, D.M. Jenkins, H. Choi, J.W. Kim, M. Asagiri, A. S. Cowburn, H. Abe, K. Soma, K. Koyama, M. Katoh, K. Sayama, N. Goda, R. S. Johnson, I. Manabe, R. Nagai, I. Komuro, HIF-1alpha-PDK1 axis-induced active glycolysis plays an essential role in macrophage migratory capacity, Nat. Commun. 7 (2016) 11635.